Tunable Se vacancy defects and the unconventional charge density wave in $1T$-$TiSe_{2-\delta}$

S. H. Huang,[1,2] G. J. Shu,[1] Woei Wu Pai,[1] H. L. Liu,[2] and F. C. Chou[1,3,4,*]

[1]*Center for Condensed Matter Science, National Taiwan University, Taipei 10617, Taiwan*

[2]*Department of Physics, National Taiwan Normal University, Taipei 11677, Taiwan*

[3]*National Synchrotron Radiation Research Center, Hsinchu 30076, Taiwan*

[4]*Taiwan Consortium of Emergent Crystalline Materials, Ministry of Science and Technology, Taipei 10622, Taiwan*

(Received 2 February 2016; revised manuscript received 6 December 2016; published 31 January 2017)

A systematic study of polycrystalline $1T$-$TiSe_{2-\delta}$ with controlled Se loss indicates that the unconventional charge density wave (CDW) phase is found to be most pronounced in samples with $\delta \sim 0.12$, instead of being Se vacancy free. The level of Se vacancy defects and temperature determines whether $1T$-$TiSe_{2-\delta}$ should be categorized as a semiconductor, a semimetal, or an excitonic insulator. An interpretation using a general band picture of p-type doped narrow-band-gap semiconductor with an impurity band (IB) in proximity to the valence band (VB) is proposed to explain the evolution of electronic structures for $1T$-$TiSe_{2-\delta}$, from the intermediate doping of $\delta \sim 0.08$, to the critical doping of $\delta \sim 0.12$ showing an anomalous resistivity peak between $\sim$100–200 K, and to the heavily doped of $\delta \sim 0.17$ as an n-type degenerate semiconductor. Integrated chemical analysis and physical property characterization, including electron probe microanalysis (EPMA), synchrotron x-ray diffraction, resistivity, and Seebeck coefficient measurement results are provided for the polycrystalline samples prepared via vacuum-sealed high temperature annealing route.

DOI: 10.1103/PhysRevB.95.045310

I. INTRODUCTION

The layered transition metal dichalcogenides (TMDCs) are the representative 2D materials because of their rich low-dimensional physics with great potential for battery and superconductor applications [1]. The transport behavior of $1T$-$TiSe_2$ has been shown to be highly sensitive to the growth conditions [2,3], especially when the existence of a pronounced $\rho(T)$ peak near $\sim$100–200 K has been used as the critical indicator for the crystal quality and stoichiometry [2,4–6]. Neutron diffraction studies have shown that $1T$-$TiSe_2$ undergoes a second order structural phase transition below $\sim$200 K to form a $2a \times 2a \times 2c$ superlattice of a wave vector $\mathbf{q} = (\frac{1}{2}, 0, \frac{1}{2})$ [7,8]. Although it is common to correlate the CDW phase formation with Fermi surface nesting, this may not be applicable to $1T$-$TiSe_2$ for which the parallel portion of the Fermi surface was neither predicted from band calculations nor confirmed by angle-resolved photoemission spectroscopy (ARPES) [5,9]. The physical origin of the unconventional CDW phase of $1T$-$TiSe_2$ has been gradually narrowed down to an excitonic insulator scenario, wherein an electron-hole exciton condensate occurs with softening of the phonon mode at the Γ-L zone boundary [10–15]. The phonon mode softening could be viewed as the precursor leading to the symmetry breaking of a $2a \times 2a \times 2c$ superlattice via a second order structural phase transition.

Most of the published experimental and theoretical works implied that $1T$-$TiSe_2$ is stoichiometric or with Ti excess so far, and the CDW phase has been assumed to exist in the stoichiometric compounds with the most pronounced $\rho(T)$ peak of onset $\sim$200 K [2,4,5,7,16–18]. We have performed an integrated chemical and physical property analysis on a series of $1T$-$TiSe_2$ polycrystalline samples prepared via a vacuum-sealed route at various annealing temperatures from 350 to 950 °C. It is found that the nominal $1T$-$TiSe_2$ could also exist in the form containing severe Se vacancy defects and depends strongly on the annealing temperature. In particular, the sample with the most pronounced $\rho(T)$ CDW anomaly is confirmed to occur when δ is near $\sim$0.12, instead of being stoichiometric.

II. EXPERIMENTAL DETAILS

An $1T$-$TiSe_2$ polycrystalline sample was synthesized from raw material of Ti and Se powders. The precursors with the stoichiometric molar ratio were thoroughly mixed and then sealed in an evacuated quartz tube. A prolonged heating cycle of low reaction temperature at 350 °C was chosen with repeated grinding in the glovebox and re-sealing after each heating cycle of three days. After the single phase of $1T$-$TiSe_2$ was confirmed by x-ray diffraction, the powder sample was separated into several batches and sealed in evacuated quartz tubes for post-annealing, at different temperatures ranging from 350 to 950 °C for one day each.

The crystal structure and phase purity of $1T$-$TiSe_2$ polycrystalline samples was confirmed by x-ray diffraction at room temperature using both the in-house x-ray and synchrotron x-ray ($\lambda = 0.61993$ Å) at Taiwan NSRRC. An electron probe microanalyzer (EPMA) was used for the chemical analysis, where 10-point average was obtained from scans within mm range of cold pressed discs. Electrical resistivity, Seebeck coefficient, and Hall effect measurements were performed using a physical property measurement system (PPMS, Quantum Design) with a four-point probe method.

III. RESULTS AND DISCUSSION

A. Synthesis and defects

The x-ray diffraction patterns and refined results for four representative polycrystalline samples with confirmed single phase are shown in Fig. 1. Judging from the dark red deposit on the inner wall of the vacuum-sealed tube after high temperature annealing (inset of Fig. 2), the evaporated element at the colder

*fcchou@ntu.edu.tw

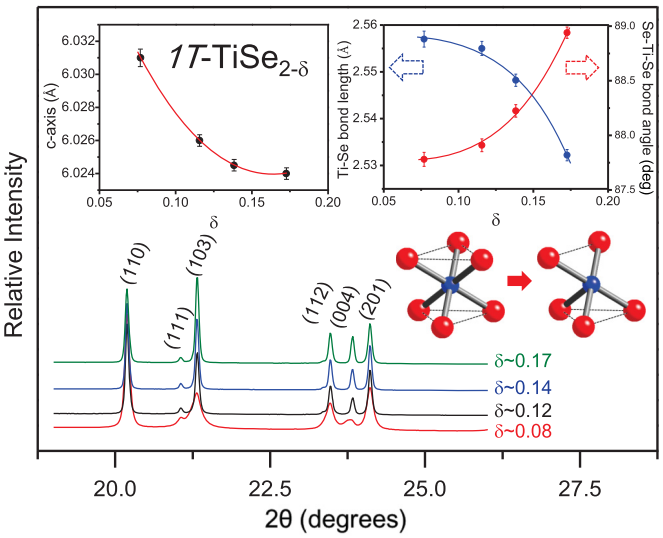

FIG. 1. X-ray diffraction (XRD) patterns for $1T$-$TiSe_{2-\delta}$ obtained using synchrotron radiation of wavelength $\lambda = 0.61993$ Å and indexed with space group $P\bar{3}m1$ (No. 164). The left inset shows the c axis and the right inset shows the bond length/angle as a function of Se vacancy level δ (solid lines are guide to eyes).

end is likely to be Se as confirmed by the inductively coupled plasma (ICP) chemical analysis. It is also observed that higher annealing temperature introduces a thicker layer of Se deposit, being consistent to the EPMA analysis of higher Se vacancy level after the controlled annealing.

When the Se deficiency level δ is plotted against the annealing temperature in an Arrhenius plot, as shown in Fig. 2, a thermally activated behavior of energy barrier Q $\sim$ 100 meV is found, which corresponds to the thermal energy k_BT of T $\sim$ 1160 K and is consistent with the experimentally estimated decomposition temperature of T $\gtrsim$ 950 °C. Such activation

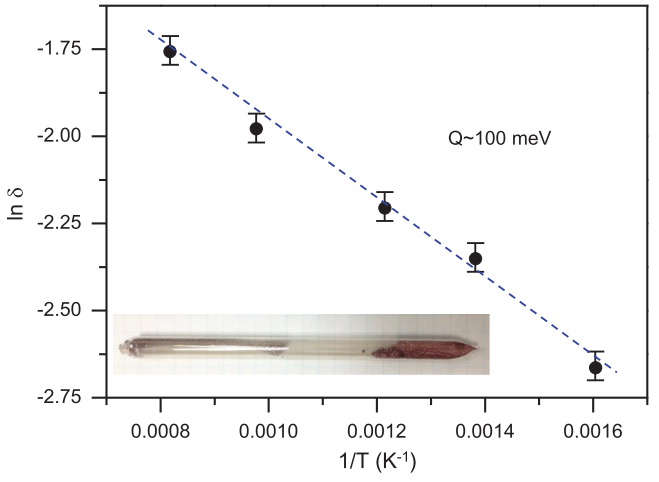

FIG. 2. An Arrhenius plot of Se deficiency level δ vs annealing temperature for $1T$-$TiSe_{2-\delta}$ powder samples, where an activation behavior of a gap ~100 meV is found to indicate the Se vacancy defect formation mechanism. A photo for the pristine powder sample sealed in an evacuated quartz tube after the high temperature annealing is also shown in the inset, where a dark red deposit of Se is found in the inner wall of the colder end.

behavior of vacancy generation is a typical thermodynamic phenomenon for the point defect formation [19], i.e., surface point defects are generated as a result of thermal energy-assisted surface Se atom escape, following the reaction of $TiSe_2 = TiSe_{2-\delta} + \frac{\delta}{2}Se_2(g)$. In fact, it is common and nearly impossible not to find intrinsic defects in the chalcogenides, which has made the definitions of "intrinsic" and "stoichiometric" controversial in the selenides [20]. Similar Se loss phenomenon has also been confirmed in the crystal growth of layered Bi_2Se_3 having Se atoms in the vdW gap between quintuple layers [21].

It is surprising to find that the pristine powder sample synthesized at low temperature near 350 °C already shows a significant amount of Se loss at the level of $\delta \sim 0.08 \pm 0.02$, even with excess Se added in the precursor mixture. Additionally, a single phase powder sample could not be synthesized at temperatures below ~350 °C following the current method, strongly suggesting that the $1T$-$TiSe_{2-\delta}$ sample prefers to contain Se vacancy defects for samples which must be prepared in the vacuum-sealed oxygen-free environment. By contrast, the maximum Se loss for $1T$-$TiSe_{2-\delta}$ was found to be near $\delta \sim 0.17$ by vacuum-sealed annealing at 950 °C, prior to reaching the quartz tube softening temperature limit. It is also found that Se loss approaches a saturated level near 950 °C before an impurity phase is observed. All these experimental results point to the existence of pure $1T$-$TiSe_{2-\delta}$ phases with various Se vacancy defect levels in the range of $\delta \sim 0.08$–0.17.

Based on defect studies of $1T$-$TiSe_2$ with scanning tunneling microscopy and spectroscopy (STM/STS), Hildebrand *et al.* proposed that at least three types of defect exist, including intercalated Ti atoms, Se vacancies, and Se substitutions by residual iodine and oxygen atoms [22]. STM study with model calculations also showed a consistent picture supporting the existence of intercalated Ti in the vdW gap [23]. On the other hand, we note that in order to produce single crystal samples with a pronounced CDW anomaly peak in $\rho(T)$ near 200 K, a prolonged high temperature annealing procedure has been applied, could be required by the much longer diffusion length for the single crystal ($\gtrsim$1 mm), comparing to the powder sample of smaller grain size (~10–30 μm). It is possible that the prolonged annealing time (as long as three weeks [2]) may have promoted local structure re-construction near the Se-vacancy sites to assist the $TiSe_{2-\delta} \Longrightarrow (TiSe_2)(Ti_{1+x}Se_2)$ phase segregation, especially near the surface regime having a higher density of Se vacancies. While no chemical analysis data are available to those single crystal samples used in early works, it is unclear whether there actually exist two types of *homogeneous* single crystal of $1T$-$TiSe_2$ with either Ti-excess or Se-deficiency in the bulk, a parallel study using single crystals with controlled annealing temperature and time length is required. Here, we report the chemical and physical property measurement results on a series of polycrystalline samples with controlled Se vacancy levels, which is expected to correlate the defect-dependent physical properties to the homogeneous bulk stoichiometry more consistently.

B. Crystal structure and defects

The Se vacancy defects in polycrystalline samples of $1T$-$TiSe_{2-\delta}$ do not introduce additional impurity phases, as

confirmed by the high resolution synchrotron x-ray (Fig. 1) and the magnetic susceptibilities (not shown). Based on the synchrotron x-ray diffraction crystal structure refinement, a slight a-axis increase (not shown) with concomitant c-axis reduction for increasing δ is shown in the left inset of Fig. 1. The Ti-Se bond length and Se-Ti-Se bond angle in the tilted TiO_6 octahedron (equivalent to a trigonal antiprism) as a function of δ are also presented in the right inset of Fig. 1. It is found that Ti-Se bond length is shortened with concomitant Se-Ti-Se bond angle increase for samples of higher Se deficiency level in average. The observed trend of bond length/angle changes with increasing δ is opposite to the predicted bond length changes of Ti-Se and Se-Se for $1T$-$TiSe_2$ having intercalated Ti in the vdW gap [24]. On the other hand, the observed trend of bond length/angle changes is in agreement with the impact of reduced coordination number (CN) to the local structure, e.g., similar bond length/angle variation has been found in iron crystal moving from the structure of face-centered cubic (fcc CN=12) to body-centered cubic (bcc CN=8), which has been verified and attributed to the reduced Coulomb repulsion among ligands in the crystal electric field [25]. The shortened Ti-Se bond length and enlarged Se-Ti-Se bond angle in average with increasing δ can thus be interpreted consistently due to the loss of Se that reduces the coordination number from $TiSe_6$ of CN=6 to $TiSe_5$ of CN=5 in average, as illustrated in the lower right inset of Fig. 1. The observed local structure variation is also consistent to the expected thinner Ti-Se trilayer in average and the observed c-axis reduction (left inset of Fig. 1). By contrast, the nominal $TiSe_2$ with confirmed intercalation of transition metal element Cu showed c-axis increase, presumably as a result of enlarged average vdW gap size [26].

C. Transport properties

The resistivities as a function of temperature for polycrystalline samples $TiSe_{2-\delta}$ with $\delta \sim 0.08$, 0.12, 0.14, and 0.17 are shown in Fig. 3(a). While many earlier works reported samples of the most pronounced $\rho(T)$ peak anomaly near 100–200 K to be stoichiometric with high quality [2,4,27], it is surprising to find that the pristine sample having the lowest Se deficiency level of $\delta \sim 0.08$ shows a typical semiconducting behavior, with only an insignificant trace of $\rho(T)$ peak anomaly near ~200 K. In fact, the CDW anomaly is masked by the high resistivity background and can only be identified by the magnetic susceptibility measurement (not shown) more clearly. In addition, the most pronounced $\rho(T)$ peak (defined with $\rho_{peak}/\rho_{valley}$ following Refs. [2,4,5]) is confirmed to occur at a critical level of $\delta \sim 0.12$, instead of being stoichiometric. The $\rho(T)$ peak could appear on two different kinds of background of either semiconducting or metallic character [see dashed lines in Fig. 3(a)] with a metal-insulator background crossover between $\delta \sim 0.12$–0.14. Current results indicate that the anomalous $\rho(T)$ peak size depends strongly on the δ level. Aside from the $\rho(T)$ peak anomaly, the electronic character of $1T$-$TiSe_{2-\delta}$ is shown to evolve from the typical semiconductorlike behavior to the metallic behavior from $\delta \sim 0.08$ to 0.17.

To further explore the δ and temperature dependencies of carrier characteristics, Seebeck coefficient measurement

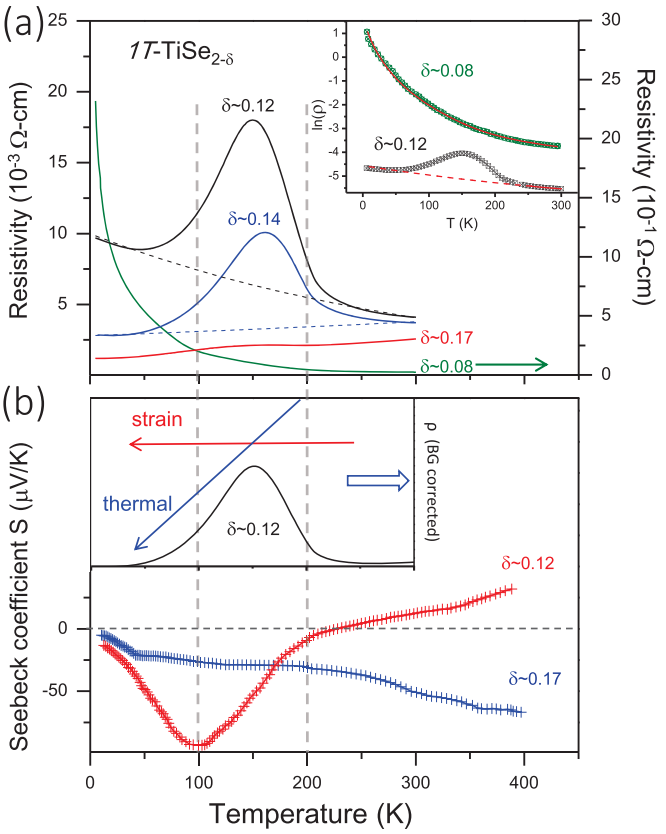

FIG. 3. Temperature dependence of (a) electrical resistivity and (b) Seebeck coefficient for $1T$-$TiSe_{2-\delta}$. The background of $\rho(T)$ (in dashed lines) evolves from a semiconducting to metallic behavior with increasing δ. The inset of (a) shows how activation energy E_a is estimated from the ln ρ vs T plot via an $\exp^{-\frac{E_a}{k_B T}}$ fitting. Note the data near CDW peak anomaly are skipped for the fitting of $\delta \sim 0.12$. The inset of (b) illustrates how the $\rho(T)$ anomaly of $\delta \sim 0.12$ is shaped by the competing thermal and strain energies after the semiconducting background subtraction.

results for $1T$-$TiSe_{2-\delta}$ are shown in Fig. 3(b). The carrier sign change from p to n type occurs near ~200 K for $\delta \sim 0.12$, and the $\delta \sim 0.17$ shows persistent n-type character for the whole temperature range. The p-to-n-type change near ~200 K for $\delta \sim 0.14$ of metallic background [Fig. 3(a)] has also been confirmed with Hall measurement (not shown), and the carrier concentration and mobility estimated from the Hall effect measurement are shown in Table I. Similar observations have also been reported by Di Salvo *et al.* on a nominal $TiSe_2$ sample showing pronounced $\rho(T)$ peak on a metallic background, and the two-band model analysis showed higher density of holes [7]. Fitting the resistivity data between 5–300 K for $\delta \sim 0.08$, and the data for $\delta \sim 0.12$ between 250–300 K

TABLE I. Carrier concentrations and mobilities derived from resistivity and Hall effect measurement results for $\delta \sim 0.14$.

T(K)	n(cm^{-3})	R_H(cm^3/Coul)	μ(cm^2/V-S)
5	1.49×10^{20}	−0.0419	15
300	2.56×10^{20}	0.0244	7

TABLE II. The activation energy E_a of $1T$-$TiSe_{2-\delta}$ estimated from $\rho(T)$, as shown in the inset of Fig. 3(a).

δ	E_a(meV)	CDW onset (K)	transport behavior
0.08	30 ± 2		semiconducting
0.12	16 ± 2	198 ± 2	semiconducting
0.14		193 ± 3	metallic
0.17			metallic

to avoid CDW phase contamination [inset of Fig. 3(a)], semiconducting transport behavior following the activation law of e^{-E_a/k_BT} were found with activation energy E_a values summarized in Table II. The band gap size indicated by the E_a value is reduced from ~30 meV ($\delta \sim 0.08$) to ~16 meV ($\delta \sim 0.12$) as a result of heavier doping from more Se vacancy defects.

Interestingly, the magnitude (absolute value) of the Seebeck coefficient for $\delta \sim 0.12$ increases at the CDW phase onset near ~200 K and reaches a maximum near ~100 K [see Fig. 3(b)]. Since the magnitude of the Seebeck coefficient reflects the effect of carrier diffusion as a result of its coupling to the crystal structure, i.e., the phonon drag phenomenon is closely related to the CDW state formation [28], the increasing magnitude of the Seebeck coefficient for $\delta \sim 0.12$–0.14 between 100–200 K is consistent with the range of CDW phase formation revealed by the sharp $\rho(T)$ anomaly [Fig. 3(a)]. These results support the second order nature of the structural phase transition from neutron diffraction [7] and the scenario of CDW phase formation via exciton-phonon-driven charge ordering [12].

D. Semiconductor or semimetal?

Many studies viewed the nominal $1T$-$TiSe_2$ as a semimetal with an indirect band overlap between Γ and L points above ~200 K [4,5]. In addition, the metal-to-insulator transition near the onset of CDW phase ~200 K has been interpreted in many ways in the literature, including as a transition from a semimetal to a state of excitonic condensation [5], from a semimetal to a CDW phase of unusual band-type Jahn-Teller effect [16], or from a semimetal to a semimetal with exciton formation [29]. However, Rasch *et al.* have designed an ARPES experiment to examine the band gap allowing the detection of thermally excited electrons above the Fermi level at room temperature [30]. The study showed that water was adsorbed on the surface to lower the conduction band via band bending and that there was a definitive band gap of $E_g \sim 150 \pm 20$ meV at room temperature, i.e., the ideal $1T$-$TiSe_2$ should be categorized as a semiconductor, as also suggested by the Ti($3d$)-Se($4p$) p-d gap calculations for an ideal $TiSe_2$ with relativistic corrections [31,32]. We believe that on the classification of a sample via temperature dependence of resistivity, caution must be taken on samples having a narrow band gap which is smaller than the thermal energy at room temperature ($k_BT \sim 26$ meV). Above all, the calculated band structure describes a $T = 0$ picture without thermal excitation.

Based on the ionic model prediction, Se vacancy defect formation is expected to create an n-type doping following the Kroger-Vink notation of $Se^{2-} = V_{Se}^{\cdot\cdot} + Se(g)$ [33], however, the carrier type has been confirmed to be p type by the positive Seebeck coefficients for $\delta \sim 0.12$ above ~200 K, as shown in Fig. 3(b). For the heavily doped p-type narrow band gap semiconductor, the doped carriers can be depicted by an impurity band (IB) sitting right above the valence band (VB) [34]. In particular, narrow gap semiconductors are strongly dependent on both the doping level and temperature, especially when the narrow gap size is lower than the thermal energy near room temperature ($k_BT \sim 26$ meV at 300 K). The samples of $\delta \sim 0.12$ having a narrow gap ~16 meV (Table II) fall into this category critically, not to mention that the narrow gap size of ~16 meV (~186 K) becomes sensitive to the electron-phonon coupling indicated by the onset of CDW phase near ~200 K, which could be part of the reason why material classification of the nominal $1T$-$TiSe_2$ is so controversial [5,30], especially when the carrier doping from Se vacancy defect or even Ti excess is ignored.

We believe that in order to interpret the transport properties and ARPES spectra of a system having a narrow gap or a narrow band overlap at room temperature rigorously [35], it is absolutely necessary to match the defect level for the samples used on experimental data taking, as already suggested by J. A. Wilson before [36]. In addition, on the definition of an excitonic insulator, Jérome *et al.* have pointed out that either a semiconductor with very narrow band gap or semimetal of small band overlap is possible, which has been examined fully on the BCS-type theoretical development and the proposal for the experimental realization [37]. It would be too hard to separate the origin of the free-carrier contributions masked by the defect self-doping effect and thermal excitation [22], especially for the semiconductor of a very narrow band gap and the semimetal of a very narrow band overlap. Current work has demonstrated the important role of defects played in the study of excitonic insulator also.

E. Band picture description

Based on the experimental results showing $1T$-$TiSe_{2-\delta}$ as a p-type semiconductor of intermediate to high doping level, we may describe the electronic characteristics of samples in the range of $\delta \sim 0.08$–0.17 using a general band picture phenomenologically. Following the proposal by Rasch *et al.* on categorizing the undoped $1T$-$TiSe_2$ without thermally excited electrons as a semiconductor of $E_g \sim 150$ meV [30], we believe the sample of $\delta \sim 0.08$ is intermediately doped as a p-type semiconductor of $E_a \sim 30$ meV (Table II), as illustrated by a narrow impurity band (IB) above the valence band (VB) shown in Fig. 4(a). The increased doping to $\delta \sim 0.12$ creates a narrower gap of $E_a \sim 16$ meV (Table II), which becomes critical and extremely sensitive to the thermal excitation near room temperature (300 K $\sim k_BT = 26$ meV), and the excitonic excitation via electron-hole coupling across the narrow gap assists the CDW instability near ~200 K through electron-phonon coupling [7], as illustrated in Fig. 4(b). Finally, the heavily doped $\delta \sim 0.17$ has an impurity band so broad that the system becomes indistinguishable between an n-type degenerate semiconductor or a metal (semimetal), as illustrated in Fig. 4(c).

While the resistivity increase below ~200 K has been explained reasonably well within the context of an un-

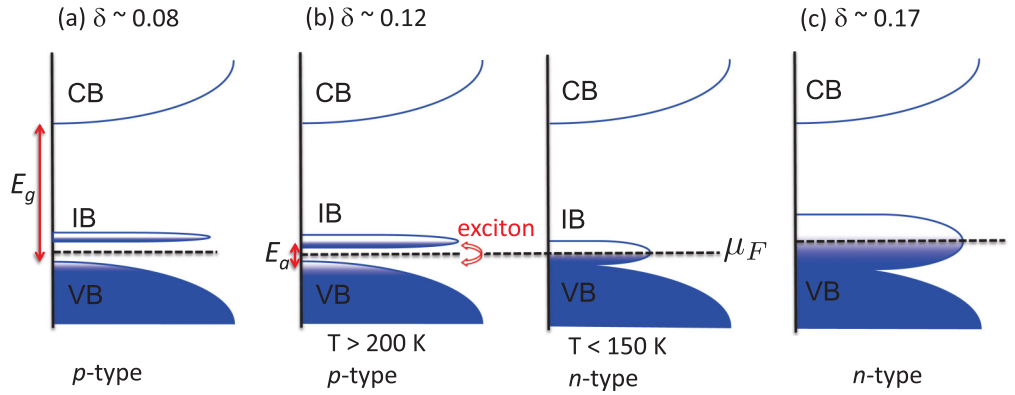

FIG. 4. Band pictures of $1T$-$TiSe_{2-\delta}$. (a) $\delta \sim 0.08$ as a p-type semiconductor of a band gap E_g between the conduction band (CB) and the valence band (VB) with intermediate level of acceptors aggregated to form an impurity band (IB) above VB. (b) $\delta \sim 0.12$ as a p-type semiconductor of a critical doping level that contains excitonic conduction mechanism across a very narrow band gap ($E_a \sim 16$ meV) between IB and VB. The narrow gap in $\delta \sim 0.12$ is closed again below $T \sim 150$ K to become n type, as a result of strain-induced impurity band broadening. (c) $\delta \sim 0.17$ as a heavily doped n-type degenerate semiconductor.

conventional CDW phase formation or charge ordering with concomitant exciton-phonon coupling in the literature [12,38–40], the additional resistivity drop below ~150 K and the Seebeck coefficient p-to-n type change near ~200 K remains a puzzle. Here, we propose a tentative explanation by treating $1T$-$TiSe_{2-\delta}$ of $\delta \sim 0.12$ as a p-type narrow band gap semiconductor having two types of conduction mechanism, including the excitonic excitation and the introduction of free carriers via thermal excitation. As the superlattice structure of $2a \times 2a \times 2c$ is building up gradually on cooling via a second order phase transition near ~200 K [4], resistivity increases to reflect the charge ordering indicating the existence of a narrow band gap at the order of 200 K ($k_B T \sim 17$ meV). However, the resistivity is reduced again with concomitant p-to-n carrier type change between ~150–100 K, which implies that the narrow gap of $E_a \sim 16$ meV (Table II) is closing up, as illustrated in Fig. 4(b). The closing of the narrow band gap at temperatures below ~150 K could be assisted by the strain-induced impurity band broadening to convert the p-type system into n-type, similar to the heavily doped $\delta \sim 0.17$ of broader impurity band in n-type [Fig. 4(c)]. In principle, strain energy must be generated and stored via local structure distortion to induce local electronic excitation near the vacancy site, which is nearly temperature-independent and becomes dominant at low temperature when the averaging effect from the thermal fluctuation is diminished, as illustrated by the $\rho(T)$ of $\delta \sim 0.12$ after a semiconducting background subtraction [inset of Fig. 3(b)].

IV. CONCLUSIONS

In summary, phase-pure and homogeneous polycrystalline samples of $1T$-$TiSe_{2-\delta}$ with controlled Se deficiency level between $\delta \sim 0.08$–0.17 have been studied fully on both the chemical and transport property aspects. The sample with the most pronounced $\rho(T)$ CDW anomaly is confirmed to occur when δ is near ~0.12, instead of being stoichiometric. The carrier doping type and the corresponding transport behavior due to the Se vacancy formation is found extremely sensitive to both the Se deficiency level and temperature. In order to avoid the controversial material classification for the nominal $1T$-$TiSe_2$ from semiconductor to semimetal, the preparation method and defect type/level should be specified precisely through an integrated chemical and physical property analysis.

ACKNOWLEDGMENTS

F.C.C. acknowledges support from the Ministry of Science and Technology in Taiwan under Project No. MOST-102-2119-M-002-004. H.L.L. acknowledges support from Grant No. NSC-102-2112-M-003-002-MY3. We also thank the Instrumentation Center of National Taiwan University for assistance with the EPMA experiments.

[1] J. A. Wilson and A. D. Yoffe, Adv. Phys. **18**, 193 (1969).
[2] I. Taguchi, M. Asai, Y. Watanabe, and M. Oka, Physica B and C **105**, 146 (1981).
[3] R. Bhatt, S. Bhattacharya, R. Basu, S. Ahmad, A. K. Chauhan, G. S. Okram, P. Bhatt, M. Roy, M. Navaneethan, Y. Hayakawa, A. K. Debnath, A. Singh, D. K. Aswal, and S. K. Gupta, ACS Appl. Mater. Interfaces **6**, 18619 (2014).
[4] F. J. Di Salvo, D. E. Moncton, and J. V. Waszczak, Phys. Rev. B **14**, 4321 (1976).
[5] T. Pillo, J. Hayoz, H. Berger, F. Levy, L. Schlapbach, and P. Aebi, Phys. Rev. B **61**, 16213 (2000).
[6] F. Levy, J. Phys. C **12**, 3725 (1979).
[7] F. J. Di Salvo and J. V. Waszczak, Phys. Rev. B **17**, 3801 (1978).
[8] C. G. Slough, B. Giambattista, A. Johnson, W. W. McNairy, C. Wang, and R. V. Coleman, Phys. Rev. B **37**, 6571(R) (1988).
[9] K. Rossnagel, J. Phys.: Condens. Matter **23**, 213001 (2011).
[10] J. A. Wilson, Phys. Status Solidi B **86**, 11 (1978).

[11] H. Cercellier, C. Monney, F. Clerc, C. Battaglia, L. Despont, M. G. Garnier, H. Beck, P. Aebi, L. Patthey, H. Berger, and L. Forro, Phys. Rev. Lett. **99**, 146403 (2007).
[12] J. van Wezel, P. Nahai-Williamson, and S. S. Saxena, Phys. Rev. B **81**, 165109 (2010).
[13] C. Monney, C. Battaglia, H. Cercellier, P. Aebi, and H. Beck, Phys. Rev. Lett. **106**, 106404 (2011).
[14] M. Holt, P. Zschack, H. Hong, M. Y. Chou, and T.-C. Chiang, Phys. Rev. Lett. **86**, 3799 (2001).
[15] C. Monney, H. Cercellier, F. Clerc, C. Battaglia, E. F. Schwier, C. Didiot, M. G. Garnier, H. Beck, P. Aebi, H. Berger, L. Forro, and L. Patthey, Phys. Rev. B **79**, 045116 (2009).
[16] K. Rossnagel, L. Kipp, and M. Skibowski, Phys. Rev. B **65**, 235101 (2002).
[17] O. Anderson, G. Karschnick, R. Manzke, and M. Skibowski, Solid State Commun. **53**, 339 (1985).
[18] A. N. Titov, A. V. Dolgoshein, I. K. Bdikin, and S. G. Titova, Phys. Solid State **42**, 1610 (2000).
[19] F. A. Kroger and H. J. Vink, J. Phys. Chem. Solids **5**, 208 (1958).
[20] L.-D. Zhao, S.-H. Lo, Y. Zhang, H. Sun, G. Tan, C. Uher, C. Wolverton, V. P. Dravid, and M. G. Kanatzidis, Nature (London) **539**, E2 (2016).
[21] F.-T. Huang, M.-W. Chu, H. H. Kung, W. L. Lee, R. Sankar, S.-C. Liou, K. K. Wu, Y. K. Kuo, and F. C. Chou, Phys. Rev. B **86**, 081104(R) (2012).
[22] B. Hildebrand, C. Didiot, A. M. Novello, G. Monney, A. Scarfato, A. Ubaldini, H. Berger, D. R. Bowler, C. Renner, and P. Aebi, Phys. Rev. Lett. **112**, 197001 (2014).
[23] M. V. Kuznetsov, I. I. Ogorodnikov, A. S. Vorokh, A. S. Rasinkin, and A. N. Titov, Surf. Sci. **606**, 1760 (2012).
[24] B. Hildebrand, T. Jaouen, C. Didiot, E. Razzoli, G. Monney, M.-L. Mottas, A. Ubaldini, H. Berger, C. Barreteau, H. Beck, D. R. Bowler, and P. Aebi, Phys. Rev. B **93**, 125140 (2016).
[25] W. Zhong, G. Overney, and D. Tomanek, Phys. Rev. B **48**, 6740 (1993).
[26] E. Morosan, H. W. Zandbergen, B. S. Dennis, J. W. G. Bos, Y. Onose, T. Klimczuk, A. P. Ramirez, N. P. Ong, and R. J. Cava, Nat. Phys. **2**, 544 (2006).
[27] R. Z. Bachrach and M. Skibowski, Phys. Rev. Lett. **37**, 40 (1976).
[28] C. Kittel, *Introduction to Solid State Physics* (Wiley, New York, 1996).
[29] G. Li, W. Z. Hu, D. Qian, D. Hsieh, M. Z. Hasan, E. Morosan, R. J. Cava, and N. L. Wang, Phys. Rev. Lett. **99**, 027404 (2007).
[30] Julia C. E. Rasch, T. Stemmler, B. Muller, L. Dudy, and R. Manzke, Phys. Rev. Lett. **101**, 237602 (2008).
[31] J. Von Boehm and H. M. Isomaki, J. Phys. C **15**, L733 (1982).
[32] H. Isomaki and J. Von Boehm, J. Phys. C **14**, L75 (1981).
[33] F. A. Kroger and H. J. Vink, Solid State Phys. **3**, 307 (1956).
[34] X. Blase, E. Bustarret, C. Chapelier, T. Klein, and C. Marcenat, Nat. Mater. **8**, 375 (2009).
[35] P. Chen, Y.-H. Chan, X.-Y. Fang, Y. Zhang, M. Y. Chou, S.-K. Mo, Z. Hussain, A.-V. Fedorov, and T.-C. Chiang, Nat. Commun. **6**, 8943 (2015).
[36] J. A. Wilson, Solid State Commun. **22**, 551 (1977).
[37] D. Jrome, T. M. Rice, and W. Kohn, Phys. Rev. **158**, 462 (1967).
[38] T. E. Kidd, T. Miller, M. Y. Chou, and T.-C. Chiang, Phys. Rev. Lett. **88**, 226402 (2002).
[39] J. van Wezel, P. Nahai-Williamson, and S. S. Saxena, Europhys. Lett. **89**, 47004 (2010).
[40] J. van Wezel, P. Nahai-Williamson, and S. S. Saxena, Phys. Status Solidi B **247**, 592 (2010).